An Aspen Plus® tool for simulation of lignocellulosic biomass pyrolysis via equilibrium and ranking of the main process variables

A.Visconti, M. Miccio,D. Juchelková

***Abstract*—**Pyrolysis of non-fossil fuels is raising a growing interest in the nowadays scenario for the alternative supply of energy, fuels and chemicals. Biomass is among the most widely available and technologically promising candidate feedstocks. For simulation purposes and process design goals, kinetic-based models promise to be quite accurate in literature; however, they are computationally intensive and, more importantly, applicable only when kinetic data are available for the specific feedstock and pyrolysis equipment. Here, a different modeling approach is followed by considering that the pyrolysis reactor is under the thermodynamic equilibrium; then, the authors take advantage of the capabilities provided by the Aspen Plus® software. Therefore, this work is focused on the development of an input-output reactor model to simulate pyrolysis of a lignocellulosic biomass and to predict the effects of the main process variables. The trends of the predicted results as a function of the process operating variables are generally in accordance with those that are experimentally evident and published in literature. A limited comparison is provided against the experimental results of Honus[25]. It has to be noted that the Aspen code could not predict the composition of the liquid residue, i.e., tar.

***Keywords*—**Biomass, Pyrolysis, Aspen Plus®, Simulation, Equilibrium, Gibbs free energy, Char

I. INTRODUCTION

Biomass-derived sources accounted for 10% of total energy production worldwide in 2009, whereas biomass was the predominant energy source for approximately 2.7 billion people facing energy scarcity [1].Presently,political and, as a consequence, technological objectives are those of making more feasible, acceptableand efficient biomass-to-energy applications: as a consequence, research is focusing more and more on them[[2],[3],[4],[5]].

The biomass conversion processes can be grouped in three main categories: thermochemical, chemical and biochemical ones. Among the thermochemical processes the most important ones are combustion, gasification, pyrolysis and, more recently, torrefaction. In the last two of the list, the leading factor is heat, which converts biomass into other substances. Pyrolysis is a modern thermo-chemical decomposition process at elevated temperatures in the absence of oxygen, i.e., in an inert atmosphere. This process is now being used quite heavily in the chemical industry, for example to produce methanol, activated carbon and char from wood or coke from coal; anyway, besides the solid residue called char also valuable gaseous and liquid products are obtained with pyrolysis. The char is usually referred to as the mass of solid remaining after the pyrolysis, including both that coming from the reactor and that captured in the particle separator (Fig. 1), i.e., cyclone or filter.The gas contains mostly H_2, CO, CO_2, H_2O and CH_4, whereas the liquid, usually called bio-oil, is a complex mixture of hydrocarbons. A simplified process scheme for biomass pyrolysis is in Fig. 1.

There is some confusion in literature about the meaning of the word “bio-oil”, for which it is possible to find different synonyms (tar, pyrolytic liquids, bio-crude, etc.). The most used definition of tar refers to the whole liquid fraction, that is, organic compounds + pyrolytic water + feedstock moisture (see[5]). Pyrolytic gas mixed to the carrier gas is obtained once the bio-oil is removed in the condensers (Fig. 1).

At the heart of a pyrolysis process there is the reactor. Although it probably represents only about 10-15% of the total capital cost of an integrated system, most of research and development has focused on testing and developing different reactors on a variety of feedstocks.

The most popular technological options for the pyrolysis reactor are the bubbling fluidized bed (BFB), the circulating fluidized bed (CFB), the transported bed, the fixed bed (FB), the rotating cone [6], the ablative reactor [8], the screw and the auger reactors [8]. Some authors, while looking at the results got with biomass gasification, have also investigated the effect of some common catalysts like the nickel-based ones [10].

Vegetative or lignocellulosic biomass, also known as phytomass, is composed primarily of cellulose, hemicellulose and lignin, along with lesser amounts of extractives (e.g., terpenes, tannins, fatty acids, oils and resins), moisture and mineral matter [11].

Several research groups studied the pyrolysis of biomass on the basis of those three main components.

A. Viscontiis a scholarship holder at theDepartment of Industrial Engineering of the University of Salerno. He has been a visiting Erasmu student at Faculty of Mechanical Engineering, Department of Energy VŠB - Technical University of Ostrava (CZ).E-mail: alexandrus89@hotmail.it

M. Miccio is Associate Professor at theDepartment of Industrial Engineering of the University of Salerno, Via Giovanni Paolo II, 132 – 84084 Fisciano (SA), ITALY. He is the corresponding author with phone: +39-089-964148; fax:+39-089-968781; e-mail: mmiccio@unisa.it

D. Juchelková is the Head of theDepartment of Energy, Faculty of Mechanical Engineering, ,VŠB - Technical University of Ostrava, 17. listopadu 15, Ostrava –Poruba, CZECH REPUBLIC. E-mail:dagmar.juchelkova@vsb.cz

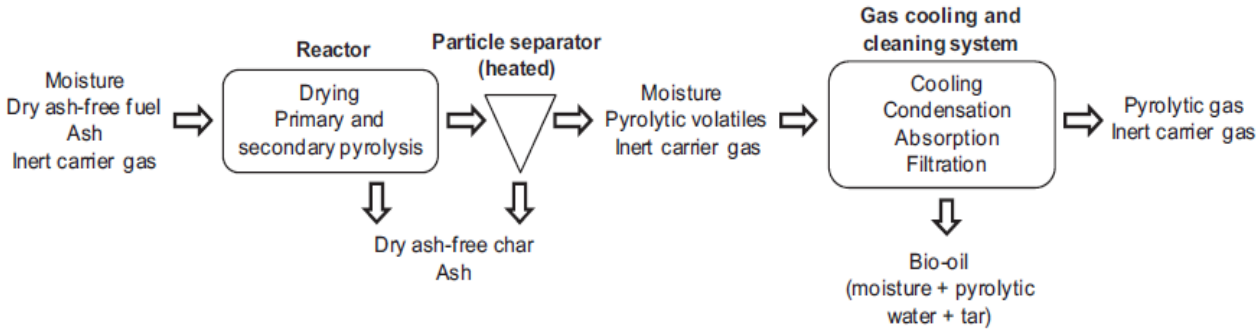

Fig. 1: simplified process scheme for biomass pyrolysis.

Raveendram et al. [12] investigated the pyrolysis characteristics of biomass components in a thermogravimetric analyzer and a packed-bed pyrolyzer;they found no detectable interactions among the components during pyrolysis in each experimental setup.Yang et al. [13] also observed negligible interactions among the three biomass components in their study, when using a thermogravimetric analyzer. On the other hand, Worasuwannarak et al. [14] studied the pyrolysis behavior of cellulose, xylan, lignin and mixtures by TG-MS technique and observed significant interactions between cellulose and lignin that caused a suppression of liquid product formation and an increase in the yield of solid residue. Wang et al. [15] also reported cellulose-lignin interactions, as well as hemicelluloses-lignin interactions, while they reported that hemicelluloses and lignin did not seem to affect each other during pyrolysis in a thermogravimetric analyzer. More recently, Wang et al. [16] studied the interactions of the biomass components in both a TG-FTIR and an experimental pyrolyzer. When using mixtures of the biomass components, they reported no significant differences between the experimental and calculated TG/DTG curves, but differences in the evolution curves of the main products (levoglucosan, 2-furfural, acetic acid and 2,6-dimethoxy phenol) were apparent. In addition, the mixed samples exhibited a common tendency to form less liquid and more gas products than what the calculations predicted. So, although these studies did not prove the complete independence of the three main biomass components on each other during thermal degradation, many authors studied the pyrolysis of hemicelluloses, cellulose and lignin individually and some of them proposed kinetic schemes as a compromise capable of describing satisfactorily the pyrolysis of a variety of biomasses [17],[18],[19],[20],[21],[22].

II. PROBLEM FORMULATION

Aspen Plus®[23] is a comprehensive chemical process modelling system, used by both academy and industry, for design, simulation, process improvement and optimization.Aspen Plus®[23]has advanced and dedicated functionalities, such as detailed heat exchanger design, dynamic simulation, batch process modelling. It also has a facility for using an equation-based approach in some of its routines, which permits convenient use of design specifications in process modelling.

In this work, the simulation of the steady-state, continuous pyrolysis of a lignocellulosic biomass feedstock has been attemptedvia Aspen Plus®. Precisely, the description of pyrolysis follows anequilibrium-based,non-stoichiometric approach, that is, no particular reaction is specified. Apart from pyrolysis, a number of elementary steps are identified and represented as model blocks for simplified process simulation (Fig. 2).

These are the main assumptions on which this model is based:

- The blocks are implicitly considered to be zero-dimensional and are regarded as perfectly insulated (e.g., the heat losses are neglected).
- Perfect mixing and uniform temperature are assumed in each block
- Residence time is long enough to reach the thermodynamical equilibrium in the reaction blocks.
- Reaction pathways and formation of intermediates are not taken into account.

The flowsheet of the model developed with Aspen Plus® is represented in Fig. 2.

The similarity is readily noticed with the simplified scheme of pyrolysis represented in Fig. 1. In fact, in both figures, the process can be divided in two sections: the first of pyrolysis/reaction and the second of separation/recovery.

The actual reaction section, in which drying, primary and secondary pyrolysis of feedstock take place, is modelled by the first three blocks, that is, the DRYER, the DECOMP and the EQUIL in Fig. 2. Actually, they are just three reactor blocks from the reactor library of Aspen Plus®.

The first block called DRYER is an “RStoic block”, takes as input the wet biomass, named FEED, and simulates the drying stage. This block requires that the amount of removed water (per unit mass of total feed, excluding inerts) must be specified.

The second block, called DECOMP, is an “RYield block” and takes as input the dried biomass, named

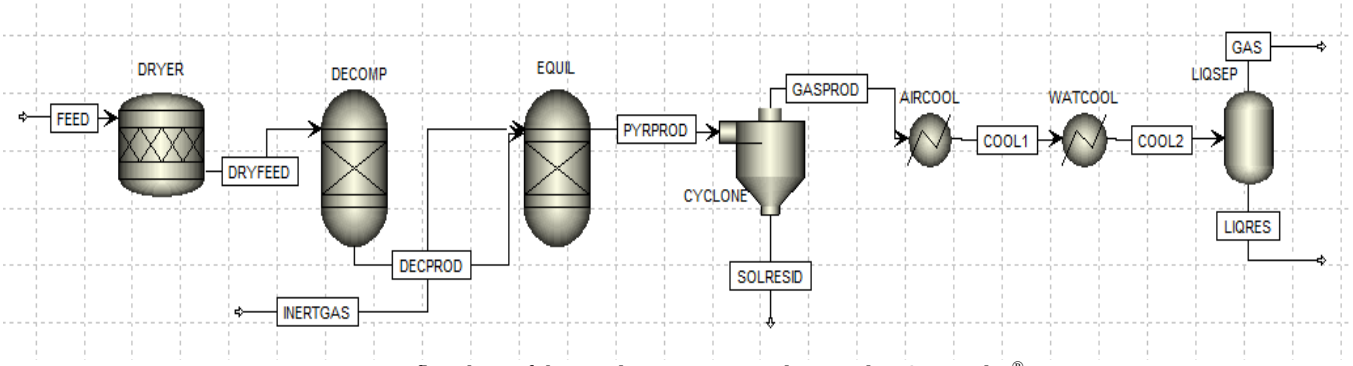

Fig. 2: flowsheet of the pyrolysis process implemented in Aspen Plus®.

DRYFEED. This block requires that the yields of the products (per unit mass of total feed, excluding any inert components) must be specified. DECOMP predicts the decomposition, at fixed temperature and pressure, of the feedstock into reference components that are: C (fixed carbon), ash, H_2O, H_2, Cl_2, S, O_2 and N_2.

For each of the blocks, i.e., DRYER and DECOMP, an external, user-supplied FORTRAN subroutine carries out the mass balance calculations and supplies the right values as inputs.

The third block, which completes the pyrolysis section, is an"RGibbs block" named EQUIL. This block takes in input the decomposed biomass and the inert gas feed, named respectively DECPROD and INERTGAS. The RGibbs block uses Gibbs free energy minimization with phase splitting to calculate thermodynamic equilibrium and it does not require reaction stoichiometry. The criteria for thermodynamic equilibrium affirm that an isothermal and isobaric chemical system is at equilibrium when the Gibbs free energy is minimized. The minimization is obtained by solving a nonlinear constrained problem using a penalty function method (SUMT) [24]. Within this simulation the EQUIL block takes as input the reference componentscoming from the DECOMP block and the inert gas and, by minimizing the Gibbs free energy, it calculates the simultaneous phase and chemical equilibrium at fixed temperature and pressure; as output, there are the species that have been specified in the EQUIL block as "possible products".

The reference biomass feedstock here considered is the same tested in the pyrolysis experiments of Honus[25]. It comes from waste wood and forestry residues.Honus[25]fed it into the pyrolysis reactor in the form of pellets with particle sizes less than 20 mm. Table I shows the ultimate and proximate analysis of this biomass.

A necessary input to perform the simulation is also the sulfur analysis, with further specification of the relative quantities of pyritic, sulfate and organic sulfur. Actually, it was not available in Honus[25]; therefore, it has been supposed that the sulfur within the biomass is equally distributed among these three species. Table II reports the sulfur distribution among the three sulfuric species.

Table III summarizes the reference processing conditions of the pyrolysis model.The operating variables are the pyrolysis temperature, pyrolysis pressure, oxygen content in the inert gas stream, inert gas flow rate, temperature of the inert gas stream, biomass feed rate and feedstock chemical composition.

Table IV shows values and variation imposed to each operating variable in the simulations.

Concerning gas properties, although the status of ideal gas could be chosen because of high temperature and low pressure, the Peng-Robinson method has been preferred because it is based on a cubic equation of state, which can take in account possible non-ideal behaviors [26].

For what concerns the results predicted by the simulation, the focus has been put on the most relevant ones, which are:

- mass yields of char, tar and gas produced
- relative concentrations of CO, CO_2, H_2, CH_4 and H_2O in the pyrolysis gas
- carbon fraction in the pyrolized solids
- pollutant concentrations in the pyrolysis gas
- higher heating value of the pyrolized char
- gas lower heating value
- net heat duty to the pyrolysis reactor

Table I: ultimate and proximate analyzes of the sample of lignocellulosic biomass and other two feedstocks.

Ultimate analysis			
	wt. % d. b.		
Component	Biomass	Tyres	Brown coal
C	47.67	85.4	63.51
H	6.86	7.56	5.14
N	0.13	0.48	1.01
Cl	0	0	0
S	0.01	0.44	0.06
O	43.98	0.01	24.58
Proximate analysis			
	wt. % d. b.(except moisture)		
Component	Biomass	Tyres	Brown coal
Moisture	7.86	1.71	13.56
Volatiles	84.71	70.86	52.51
Fixed C	13.94	23.03	41.79
Ash	1.35	6.11	5.70

TableII: sulfur distribution in the sample of lignocellulosic biomass.

Sulfur analysis			
	wt. % d. b.		
Component	Biomass	Tyres	Brown coal
Pyritic S	0.0033	0.14	0.02
Sulfate S	0.0033	0.14	0.02
Organic S	0.0034	0.16	0.02

Table III: reference input data to the ASPEN® pyrolysis model.

Blocks	T (°C)	Pressure (bar)			Other inputs
DRYER	500	1			
DECOMP	500	1			
EQUIL	500	1			
CYCLONE	500	1			
AIRCOOL	300	1			
WATCOOL	40	1			
LIQSEP	40	1			
Streams	T (°C)	Pressure (bar)	Flow rate	Mole comp.	Other inputs
FEED	25	1	50 kg/h	See prox. and ult. analyses	Sizes up to 20 mm
INERTGAS	25	1	0.5 kg/min	99% N_2, 1% O_2	-

Characteristic computation times of the Aspen® code are in the order of seconds on a PC with the Windows 8.1 operating system, i7 processor and 4 Gb RAM.

III. PROBLEM SOLUTION

A. *Effect of pyrolysis temperature*

The main components of the gaseous product resulting from the simulated pyrolysis, besides nitrogen coming from the inert carrier gas, are molecular hydrogen (H_2), carbon monoxide (CO), carbon dioxide (CO_2) and methane (CH_4), while the remainder comprises mostly water (H_2O) and little amounts of heavier alkanes and alkenes.

Table IV: values of the operating variables in terms of ranges and increments.

Operating variable	Range	Increment
Pyrolysis temperature	350-750 °C	50 °C
Pyrolysis pressure	1-10 bar	1 bar
Inert gas O_2 content	1-9 % mole	1 %
Inert gas flow rate	0.1-1 kg/min	0.1 kg/min
Biomass feed rate	10-100 kg/h	10 kg/h
Inert gas temperature	25-200 °C	25 °C
Feed chemical composition	Various feedstocks	= = =

Fig. 3 reports the trend of the pyrolysis gas composition (N_2-freemole fractions) with temperature of these five leading species.

From this graph it is readily seen how the amounts of H_2 and CO increase with temperature,whereas the opposite trend is observed for CO_2, CH_4 and H_2O. This is the trend found and confirmed during several pyrolysis and gasification experiments of biomass [25]-[27].

The following well-known reactions can explain the trends exhibited in Fig. 3:

$$CH_{4(g)} + H_2O_{(g)} \leftrightarrow CO_{(g)} + 3H_{2(g)} \qquad \Delta H_r = 205.8\text{kJ/mol}$$

reaction 1

$$C_{(s)} + CO_{2(g)} \leftrightarrow 2CO_{(g)} \qquad \Delta H_r = 172.5\text{kJ/mol}$$

reaction 2

$$C_{(s)} + H_2O_{(g)} \leftrightarrow CO_{(g)} + H_{2(g)} \qquad \Delta H_r = 131.3\text{kJ/mol}$$

reaction 3

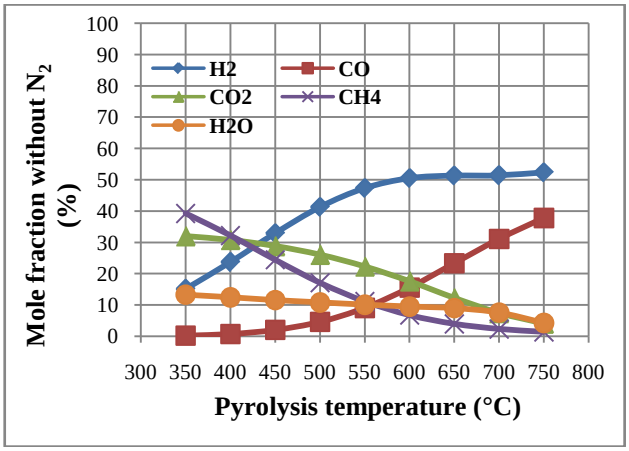

Fig.3: mole fractions of H_2, CO, CO_2, CH_4 and H_2O in the gas product as functions of pyrolysis temperature.

The first one, i.e., the “steam reforming” reaction [28], starting from methane and water, yields carbon monoxide and molecular hydrogen. The second reaction, i.e., the “Boudouard’s equilibrium” [29], describes the equilibrium between CO and CO_2 in presence of graphitic carbon. The last equation is known as “heterogeneous water gas reaction” [30]. In particular, they are all endothermic reactions and so they are favored by higher temperatures; they consume CH_4, CO_2 and H_2O to give CO and H_2.

The graphitic carbon, which can be recognized in thepyrolized char, is consumed according to reactions 2 and 3; then, it is interesting to discuss the issue of the char carbon mass fraction in the pyrolysis reactor, which has been predicted by assuming that pyrolized solidsare constituted of ashes and the carbon residueonly.

In Fig. 4 the trend of char carbon mass fraction against the pyrolysis temperature is depicted. As expected, this figure illustrates that the carbon content decreases with temperature. The important thing to notice is that, like for CO_2 in Fig. 3, the decrease of the char carbon is larger at higher temperatures, thus demonstrating that the

Boudouard equilibrium taken into account by the model is becoming relevant.

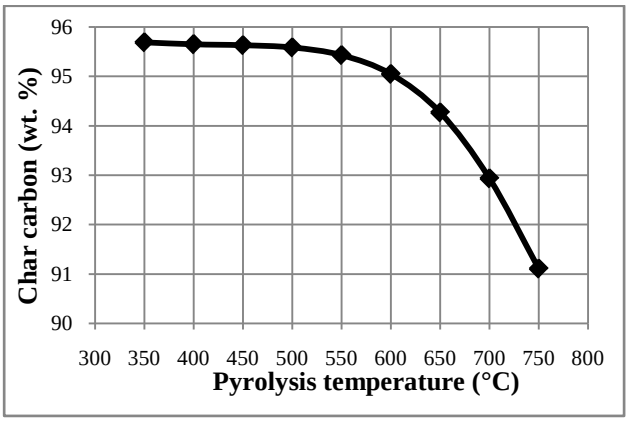

Fig. 4: char carbon mass fraction as a function of pyrolysis temperature.

As a matter of fact, one has to remember that, even if it is present in small amount, oxygen is another component of the reacting mixture and therefore there are also oxidation reactions to be considered.

The main oxidation reactions occurring within the pyrolysis gas mixture are the following:

$H_{2(g)} + 0.5O_{2(g)} \rightarrow H_2O_{(g)}$ ΔH_r = -241.8 kJ/mol
reaction 4
$CO_{(g)} + 0.5O_{2(g)} \rightarrow CO_{2(g)}$ ΔH_r = -283.0 kJ/mol
reaction 5
$CH_{4(g)} + 1.5O_{2(g)} \rightarrow CO_{(g)} + 2H_2O_{(g)}$
ΔH_r = -519.6 kJ/mol
reaction 6
$C_{(s)} + O_{2(g)} \rightarrow CO_{2(g)}$ ΔH_r = -393.5 kJ/mol
reaction 7
$C_{(s)} + 0.5O_{2(g)} \rightarrow CO_{(g)}$ ΔH_r = -110.5 kJ/mol
reaction 8

Since these are all oxidation reactions they are also exothermic and non-equilibrium reactions; anyway, reactions 7 and 8 are heterogeneous and they can be slowed down by mass transport resistances that the oxygen must overcome to come into contact with the solid carbon. The most likely pattern is that the oxidation reactions are fast enough to precede the endothermic equilibrium ones; in such a waythey consume all of the available oxygen.

The importance of the oxidation reactions grows with the oxygen content in the carrier gas; they are enhanced also by bounded molecular oxygen within the biomass feedstock itself.Nevertheless, for atypicalpyrolysis process with proper inert carrier gas, they are of minor importance.

The possible formation of pollutants has been considered as well and, among the many, the pollutants considered in the model are nitrogen monoxide (NO), nitrogen dioxide (NO_2), ammonia (NH_3), sulfur dioxide (SO_2), sulfur trioxide (SO_3) and hydrogen sulfide (H_2S). However, within the results of the simulation, appreciable quantities have been found only for NH_3, H_2S and SO_2 whereas the other pollutants quantities are negligible.

Among the many possible reactions that involve these polluting species, the most important are:

$3H_{2(g)} + N_{2(g)} \leftrightarrow 2NH_{3(g)}$ ΔH_r = -46.1 kJ/mol
reaction 9
$S(s) + H_2(g) \leftrightarrow H_2S(g)$ ΔH_r = -20.63kJ/mol
reaction 10
$4NH_3(g) + 3O_2(g) \rightarrow 2N_2(g) + 6H_2O(g)$
ΔH_r = -1267.3 kJ/mol
reaction 11
$S(s) + O_2(g) \rightarrow SO_2(g)$ ΔH_r = -296.8 kJ/mol
reaction 12

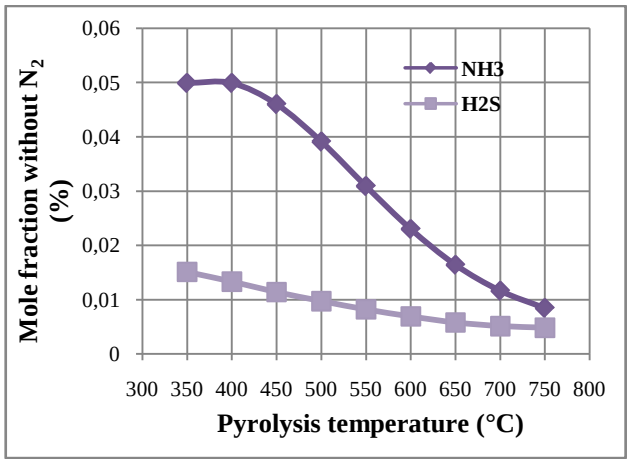

Fig. 5: NH_3 and H_2S mole fractions in the gas product as functions of pyrolysis temperature.

Fig. 5 reports the trends of NH_3 and H_2S mole fractions while Fig. 6 reports the trend of SO_2 mole fraction as functions of pyrolysis temperature.

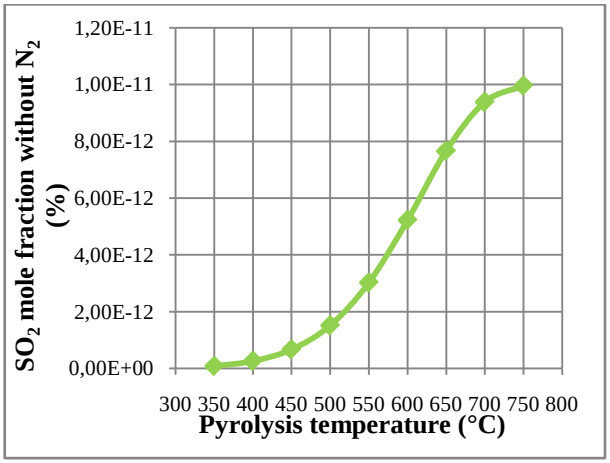

Fig. 6: SO_2 mole fraction in the gas product as a function of pyrolysis temperature.

These two figures show that the mole fractions of NH_3 and H_2S are quite small, less than 0.05%, and that SO_2 mole fraction is about nine orders of magnitude lower; nevertheless, it is still interesting to look at their trends. It can be seen that NH_3 and H_2S mole fractions decrease

with temperature and the opposite behavior is exhibited by SO_2 as a consequence of equilibrium of the two reactions 10 and 12.

Being the char a typical product ofpyrolysis, a very important parameter for its characterizationis the higher heating value (HHV), i.e.,the total enthalpy(MJ/kg)released upon combustionwhen considering the resulting water in the liquid phase.

In literature, a number of equations can be found for an approximate estimation of the heating values of different carbon-based materials, especially coals.The majority of these equations are based on the ultimate analysis of the solid under test[31]; less work had been reported with regard to lignocellulosic materials, although some equations have been proposed to estimate heating values from proximate and chemical analysis [32]-[33]-[34].

In order to estimate the higher heating value of the pyrolizedchar in the simulations, it has been chosen to utilize the equation developed by Cordero et al. [33], which is:

$$HHV = 354.3\,FC + 170.8VM \quad \text{kJ/kg} \qquad (1)$$

where FC is the fixed carbon in wt. % d.b. and VM is the volatile matter in wt. % d.b. ofthe char under test.

The trend of the char HHV with pyrolysis temperature, shown in Fig. 7, is similar to the one exhibited by the char carbon mass fraction in Fig. 4 because the above (1) is linear against it.

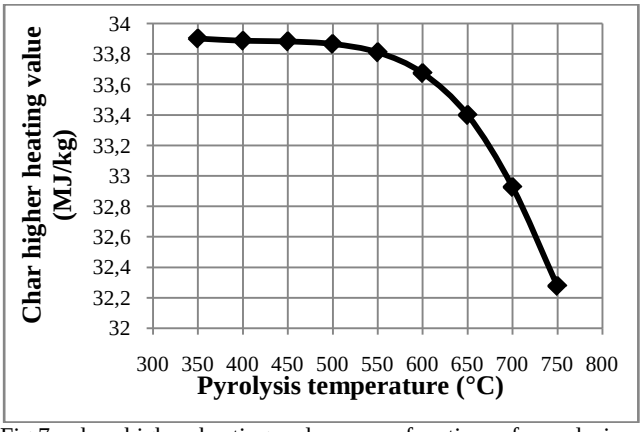

Fig.7: char higher heating value as a function of pyrolysis temperature.

As the gas composition is influenced by temperature, this also significantly affects the Lower Heating Value (LHV) of the gas product. The best way to get a LHV value as high as possible is to produce a gas enriched in CO, H_2 and CH_4, which could be suitable for energetic exploitation, for example in internal combustion engines and turbines for power production. The gas LHV has been calculated using (2), here reported [33]:

$$LHV = \left(30 * X_{CO} + 25.7 * X_{H_2} + 85.4 * X_{CH_4}\right) * 4.2 \quad \text{kJ/Nm}^3 \qquad (2)$$

whereX_{CO}, X_{H_2} and $X_{CH_4}$are the mole fractions (as calculated by considering N_2while excluding H_2O) of CO, H_2 and CH_4, respectively.

Fig. 8 shows the plot of the gas lower heating value (LHV) against pyrolysis temperature. The minimum reported for the LHV is obviously related to the previously discussed trends of CH_4, H_2 and CO. The concentration of methane, whose coefficient within (2) is the largest, decreases with temperature; this reduction is not matched by the increase of H_2 and CO and so the net effect is that of lowering LHV up to 550°C.

Above this latter T, the increase of H_2 and CO concentrations is such that LHV increases up to a maximum value of 8337 kJ/Nm^3 at 750°C.

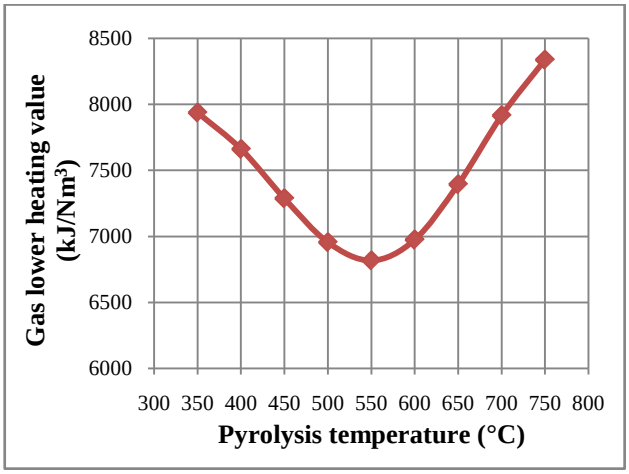

Fig. 8: gas lower heating value as a function of pyrolysis temperature.

As the pyrolysis reactor works at equilibrium, it has no size in the simulations; in particular, the heat transfer area cannot be evaluated and then the heat duty (kW) is determined just through an energy balance carried out by Aspen Plus®. Fig. 9 displays the plot of the reactor net heat duty against pyrolysis temperature and, as expected, an increasing trend is found.

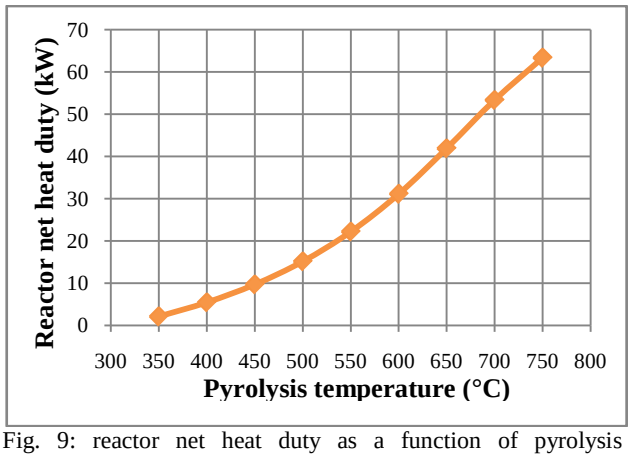

Fig. 9: reactor net heat duty as a function of pyrolysis temperature.

B. Effect of pyrolysis pressure

Fig. 10 illustrates how the values of the mole fractions (without N_2) of H_2, CO, CO_2, CH_4 and H_2O change with

pyrolysis pressure, up to P=10 bar.

H_2 and CO mole fractions decrease with a growing pressure, whereas CH_4, CO_2 and H_2O show the opposite trend; this is in contrast with what has been found by varying the pyrolysis temperature. Furthermore, analogously to what has been observed in Fig. 3 for pyrolysis temperature, the trend of H_2 is symmetric to that of CH_4 while the trend of CO is symmetric to that of CO_2. This behavior can be again explained as a consequence of the equilibrium established among the reactions 1, 2 and 3.

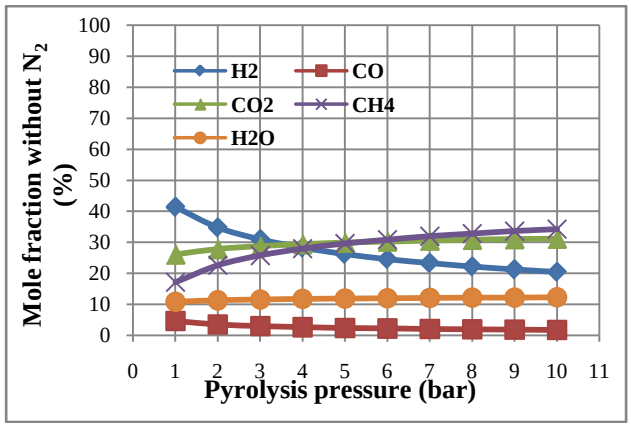

Fig. 10: mole fractions of H_2, CO, CO_2, CH_4 and H_2O in the gas product as functions of pyrolysis pressure.

Fig. 11 plots the carbon mass fraction within char against pressure.By having a look at Fig. 11, one might think that reactions 2 and 3 are not correctly taken in account because the carbon mass fraction decreases with pressure whereas solid carbonas a reactant is favored by a pressure increase. Anyway, this behavior can be explained remembering that, although to a low extent, oxidation reactions take place. It must be noted that this decrease in the char carbon with pressure is very slight, going from 95.59% at 1 bar to 95.41% at 10 bar (0.0019%).

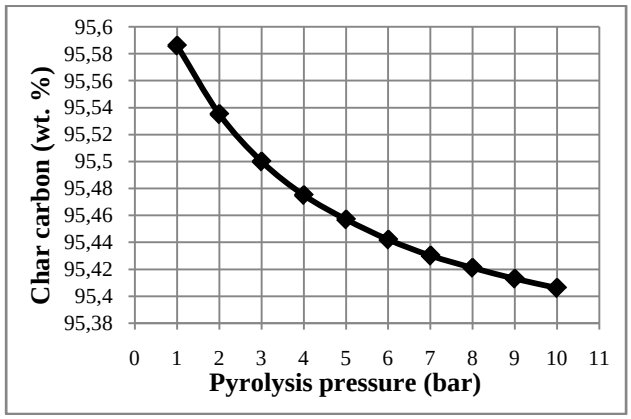

Fig. 11: char carbon mass fraction as a function of pyrolysis pressure.

Furthermore, similarly to the trends of the gaseous species mole fractions (Fig. 10), the effect of pyrolysis pressure on char carbon is more outstanding at lower pressures than at the higher ones.

Trends of the pollutants NH_3 and H_2S mole fractions as functions of pyrolysis pressure are reported in Fig.12, while SO_2 mole fraction against pyrolysis pressure is plotted in Fig.13. It is noticed that the effect of pyrolysis pressure on the pollutants is that of increasing their mole fractions. NH_3 and SO_2 experience the largest increase, achieving at 10 bar values about three times higher than those at atmospheric pressure; they shift, respectively, from 0.039% and $1{,}51*10^{-12}$ % at 1 bar to 0.1225% and $4.83*10^{-12}$ % at 10 bar; the increase of NH_3 with pyrolysis pressure ismostly explained by the mole decrease in reaction 9. The increase in H_2S, on the other hand, is by far less pronounced.

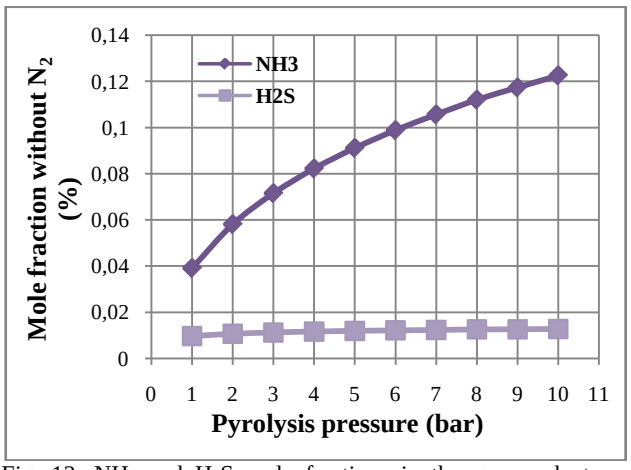

Fig. 12: NH_3 and H_2S mole fractions in the gas product as functions of pyrolysis pressure.

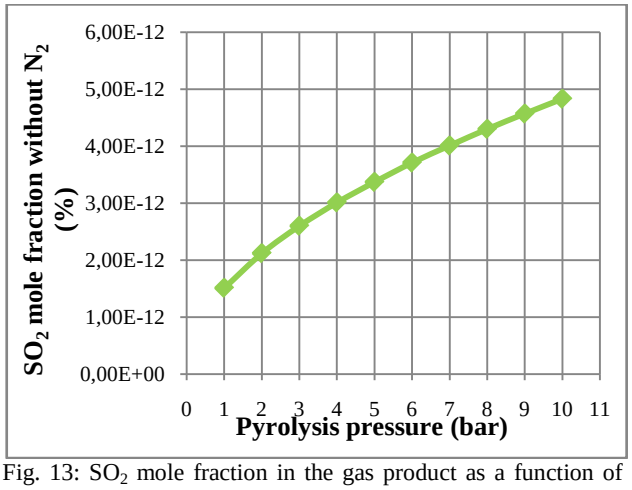

Fig. 13: SO_2 mole fraction in the gas product as a function of pyrolysis pressure.

As already noticed when studying the effect of pyrolysis temperature, pyrolysis pressure also brings about a decrease in the char higher heating value; this can be seen in Fig. 14. This reduction, anyway, is less relevant than that found with pyrolysis temperature. In fact, the char higher heating value passes from 33.87 MJ/kg at 1 bar to 33.8 MJ/kg at 10 bar, thus showing a very modest decrease (0.19%).

The lower heating value of the gas product as a

function of pyrolysis pressure is depicted in Fig. 15.

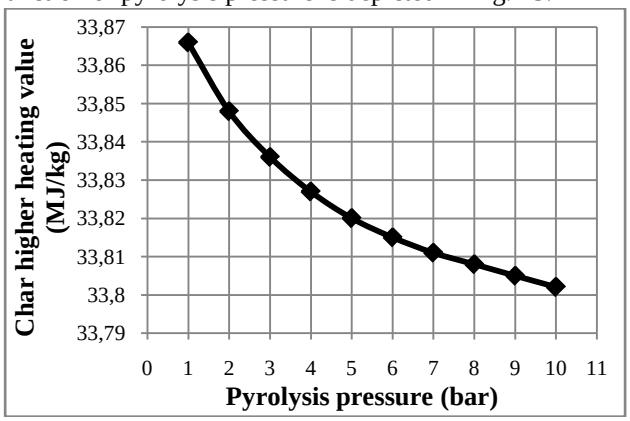

Fig. 14: char higher heating value as a function of pyrolysis pressure.

Fig. 15indicates that the gas LHV shows a monotonous increasing trend when pyrolysis pressure is raised. The increase is rather steep at lower pressures while higher ones lead to a less significant rise; since the gas LHV is computed through(2), this is mostly due to the trend of CH_4 which grows faster at lower pressure and slower at higher ones. More precisely, the increase of CH_4 mole fraction offsets the reduction of H_2 and CO mole fractions and it even brings a positive contribution to the gas LHV, which goes from 6954 kJ/Nm^3 at 1 bar to 8068 kJ/Nm^{3}at 10 bar (increase of about 16%).

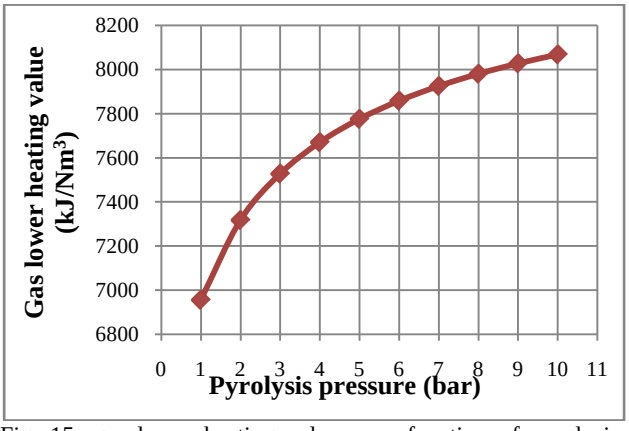

Fig. 15: gas lower heating value as a function of pyrolysis pressure.

The reactor net heat duty, plotted against pyrolysis pressure in Fig. 16, marks a consistent reduction when increasing pressure. So, an increase in the operating pressure requires less thermal energy to achieve and keep a specified temperature, with savings in terms of combustible fuels; nevertheless, this saving has to be compared with the bigger expense resulting from the necessity to compress the inert carrier gas to the required pressure and, indeed, a proper economic balance should be done.

Following the trends of all other predicted quantities, the reactor net heat duty indicates a faster change at lower pressures rather than at the higher ones.

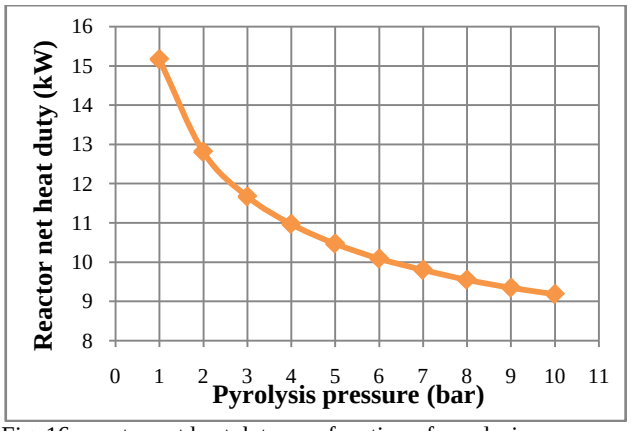

Fig. 16: reactor net heat duty as a function of pyrolysis pressure

C. *Effect of the inert gas O_2 mole fraction*

The mole fractions of H_2, CO, CO_2, CH_4 and H_2O as functions of inert gas O_2 mole fraction are represented in Fig. 17.

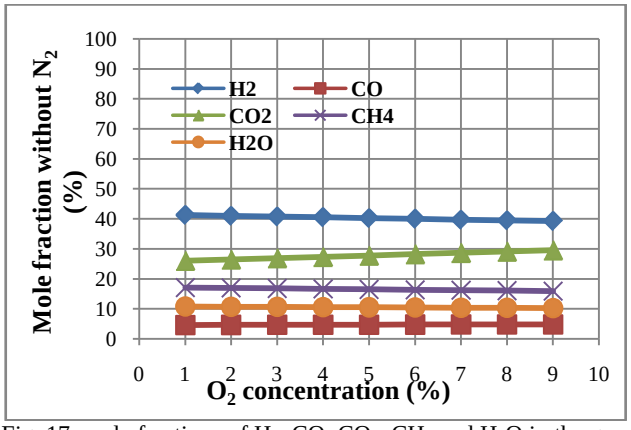

Fig. 17: mole fractions of H_2, CO, CO_2, CH_4 and H_2O in the gas product as functions of the inert gas O_2 mole fraction.

Like pressure, the effect of increasing the inert gas oxygen mole fraction is slight on the compositions of H_2, CO, CO_2, CH_4 and H_2O as well. However, H_2, CH_4 and H_2O exhibit a decrease in their mole fractions, probably due to the major extent of oxidation resulting from the larger amount of oxygen available; on the other hand, CO and CO_2 increase with a growing O_2 content in the inert gas, and this again may be ascribed to a more intense oxidative activity.

The largest variation is experienced by CO_2, which goes from 26.05% at 1% of O_2 to 29.55% at 9% of O_2 (13.4%), while the other species, in order of decreasing variation entity, are H_2, CH_4, H_2O and CO; therefore, CO seems to be the most insensitive to oxygen concentration.

As one could guess, increasing the oxygen mole fraction in the carrier gas causes a decrease of char carbon. This is shown inFig.18 and, again, can be attributed to the increased amount of oxygen that leads to an increased extent of oxidation. This reduction is linear and, like pressure, is not as relevant as that caused by pyrolysis temperature; in fact, carbon within char goes from 95.59 at 1% to 95.36 at 9%, showing a decrease of

about 0.0024%, a variation comparable to that obtained varying pressure (0.0019%).

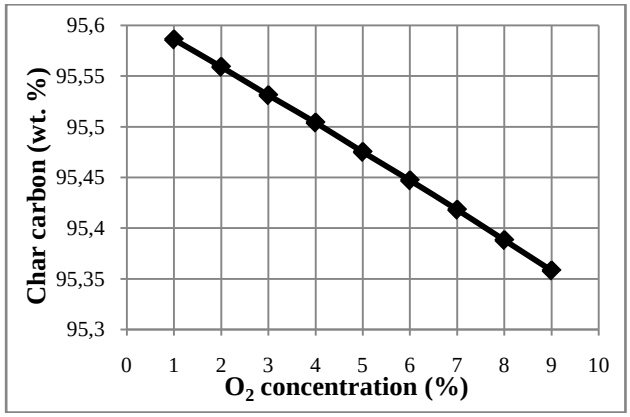

Fig. 18: char carbon mass fraction as a function of the inert gas O_2 mole fraction.

Fig. 19 reports the trends of the pollutants NH_3 and H_2S with the inert gas oxygen mole fraction whereasthe relative trend of SO_2 is shown by Fig. 20.

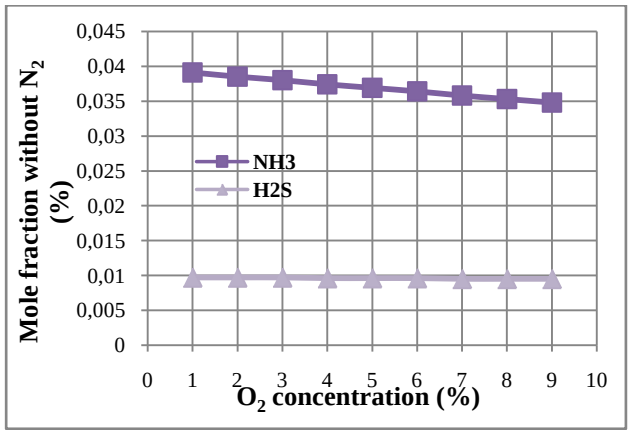

Fig. 19: NH_3 and H_2S mole fractions in the gas product as functions of the inert gas O_2 mole fraction.

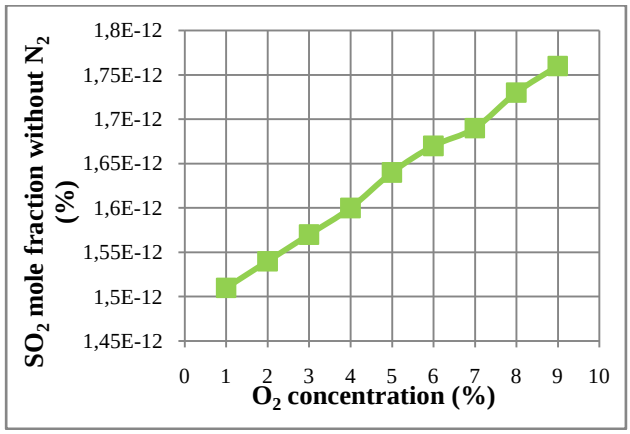

Fig. 20: SO_2 mole fraction in the gas product as a function of the inert gas O_2 mole fraction.

From Fig. 19 it can be noted that H_2S changes very little whereas NH_3 shows a decrease of its gas mole fraction. Being the result of an oxidative reaction, SO_2 (Fig. 20) undergoes an increase.

The oxygen concentration within the inert gas brings about an effect on the char higher heating value that is analogous to that of pyrolysis temperature and pressure, as it can be noticed fromFig. 21. Nevertheless, the variation is relatively small because the char higher heating value goes from 33.87 MJ/kg at 1% to 33.79 MJ/kg at 9% (a variation of only 0.24%).

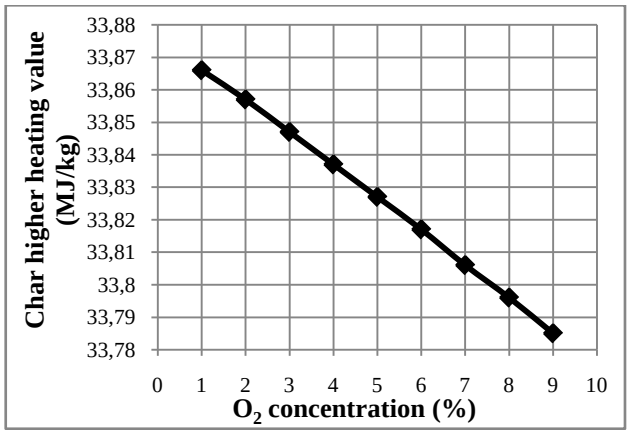

Fig. 21: char higher heating value as a function of the inert gas O_2 mole fraction.

The gas LHVas a function of the carrier gas O_2 mole fraction is depicted in Fig. 22. This diagram shows a limited, but net trend of the gas LHV to decrease when increasing the concentration of oxygen in the inert gas.If oneremembers that LHV is proportional to the amounts of H_2, CH_4 and CO present in the gas through(2), this pattern is explained by their trends already seen in Fig. 17. In fact, from this figure it has been observed that the decreases of H_2 and CH_4 are more prominent than the increase of CO; moreover, the coefficient multiplying in (2)the mole fraction of CH_4 is more than twice that multiplying the mole fraction of CO, leading to a resulting net decrease of the gas LHV with the oxygen mole content in the inert gas. In particular, the gas LHV passes from 6954 kJ/Nm^3 at 1% of O_2 to 6905 kJ/Nm^3 at 9% of O_2, a decrease of about 0.71%.

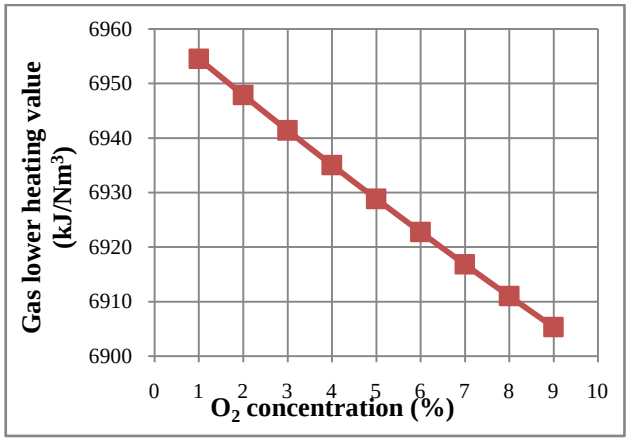

Fig. 22: gas lower heating value as a function of the inert gas O_2 mole fraction.

The reactor net heat duty has been found to

consistently decrease with the inert gas O_2 mole fraction, as reported in Fig. 23. The reason of this trend may be attributed to an increased extent of the oxidation reactions that release heat, which is in turn absorbed by the pyrolysis mixture, thus relieving the duty to be given to the reactor. This reduction in the heat duty is quite remarkable because it steps from 15.17 kW at 1% down to 5.76 kW at 9%, showing a decrease of about 62%.

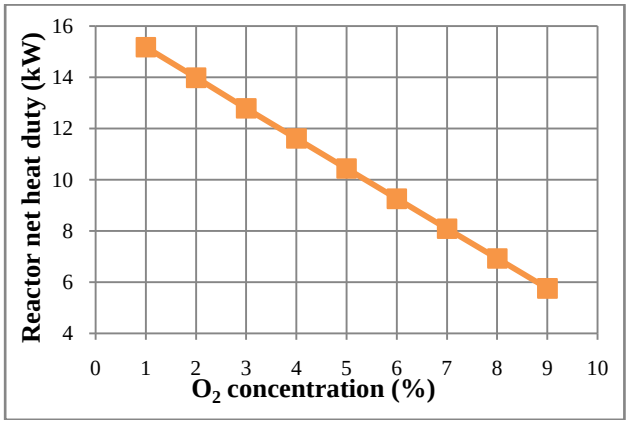

Fig. 23: reactor net heat duty as a function of the inert gas O_2 mole fraction.

D. Effect of the inert gas flow rate

Fig. 24 shows the trends of the mole fractions of H_2, CO, CO_2, CH_4 and H_2O as functions of the inert gas flow rate.

The species that exhibit a decrease in their mole fractions are CO_2 and CH_4whereas the oppositebehavior is shown by H_2, CO and H_2O. The variations of H_2, CO and CO_2 are quite slight; indeed, H_2 and CO increase respectively of the 4.27% and 19.23%, meanwhile CO_2 decrease is of 11.2%. Differently, CH_4 decreases of 32% and H_2O mole fraction almost doubles, showing an increase of about 99%. These trends can be explained considering that the increase of the inert gas causes a reduction in the partial pressures of these species because the inert gas is constituted especially of N_2; reduced partial pressures are equivalent to an increase of the reacting mixture volume and so reactions 1, 2 and 3 are shifted towards the products, that is, CO and H_2.

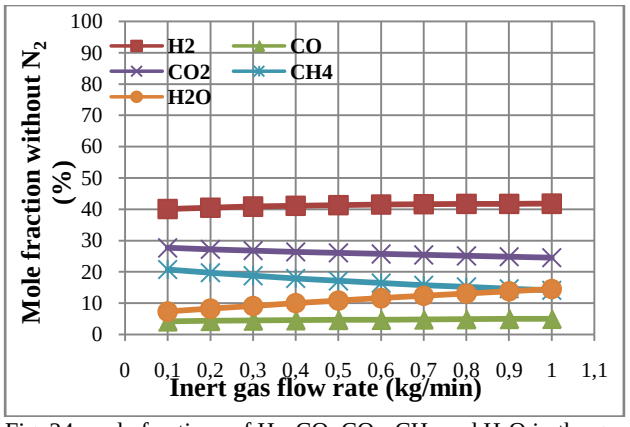

Fig. 24: mole fractions of H_2, CO, CO_2, CH_4 and H_2O in the gas product as functions of the inert gas flow rate.

The char carbon mass fraction has been plotted against the inert gas flow rate in Fig. 25. From this figure it is interesting to note that the trend of the mass fraction of the carbon within the char is not monotonous and exhibits a maximum around 0.3 kg/min; actually, the extent of the change in the char carbon mass fraction is quite limited and, hence, achieving a maximum value is not particularly significant.

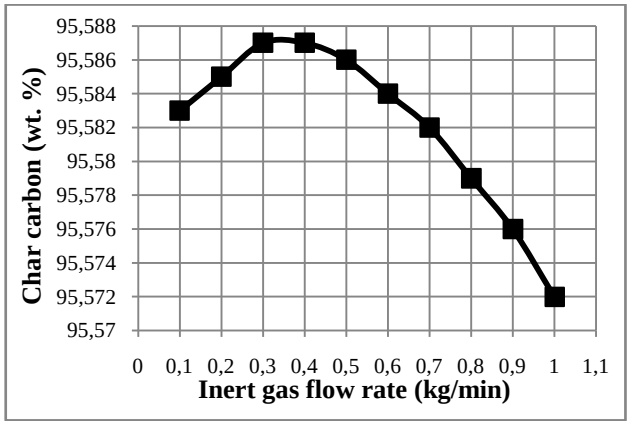

Fig. 25: char carbon mass fraction as a function of the inert gas flow rate.

Explaining this result is not so straightforward; in fact, by considering only reactions 2 and 3 and doing the same considerations done for the trends of the gaseous species, one should conclude that a monotonous decreasing trend should be observed, not the one reported in Fig. 25; this means that other heterogeneous reactions need to be considered in order to explain the relationship between the solid and gaseous phases.

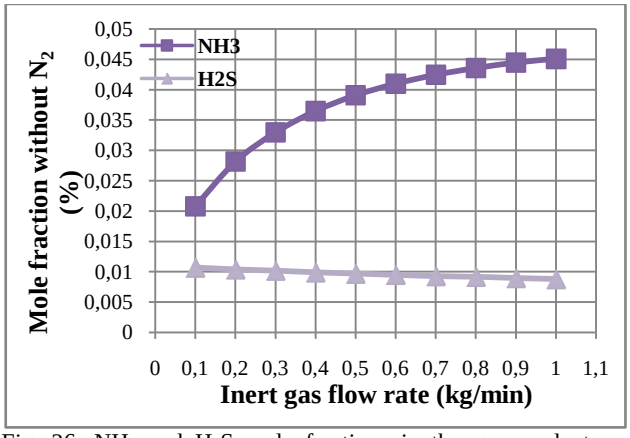

Fig. 26: NH_3 and H_2S mole fractions in the gas product as functions of the inert gas flow rate.

Fig. 26 reports the mole fractions of NH_3 and H_2S as functions of the inert gas flow rate and the mole fraction of SO_2 is plotted against the inert gas flow rate in Fig. 27. Fig. 26 indicates that the mole fraction of NH_3 experiences a steady increase, faster at lower inert gas flow rates; NH_3 mole fraction goes from 0.0208% at 0.1 kg/min to 0.0451% at 1 kg/min, an increase as high as 116.8%. In this case reaction 9 may be used to explain

the increased formation of NH_3; in fact, the increase of the inert gas flow rate makes N_2 mole fraction increase thus shifting reaction 9 towards the products.

On the other hand, H_2S mole fraction undergoes a small decrease and it passes from 0.0107% at 0.1 kg/min to 0.0088% at 1 kg/min, a decrease of about 17.8%.

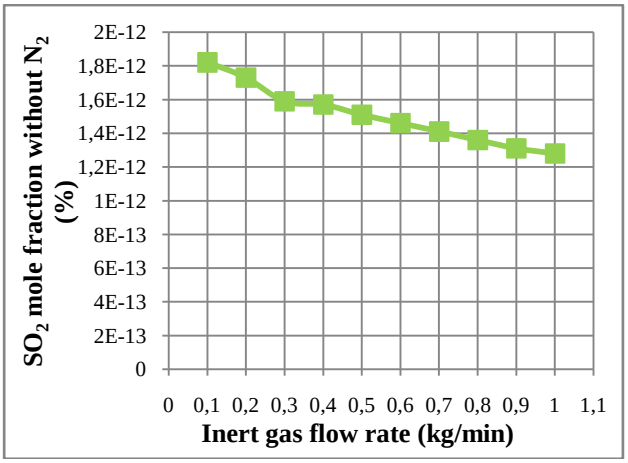

Fig. 27: SO_2 mole fraction in the gas product as a function of the inert gas flow rate.

Fig. 27 reports a reduction of SO_2 mole fraction when increasing the inert gas flow rate and this is found also for the relative molar quantity. The decrease of SO_2 mole fraction on the whole interval of variation of the inert gas flow rate is about 29.7%.

Following the trend of the char carbon mass fraction (Fig. 25) through(1), the char higher heating value displays a non-monotonous trend as reported in Fig. 28. Particularly, it increases up to a value of 0.4 kg/min for the inert gas flow rateand then it decreases. The maximum value is about 33.87 MJ/kg whereas the range of variation is very small because the difference between the maximum and the minimum value is about 0.02%.

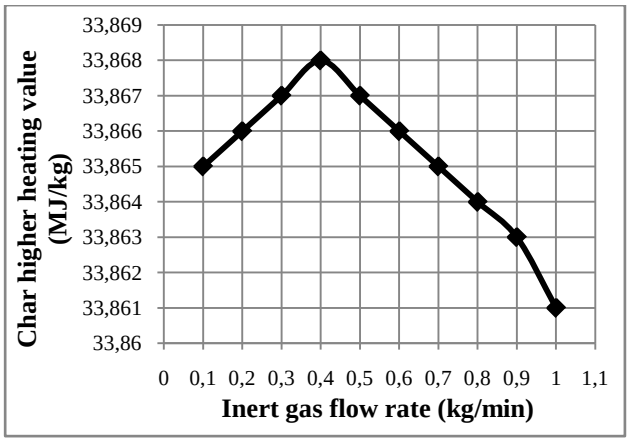

Fig. 28: char higher heating value as a function of the inert gas flow rate.

As expected, increasing the inert gas flow rate leads to larger and larger amounts of N_2 that dilutes the resulting gas product, thus lowering the gas lower heating value, as shown in Fig. 29.

It can be noticed that this decrease is more prominent at lower inert gas flow rates and it seems that a limiting value is obtained at higher inert gas flow rates.

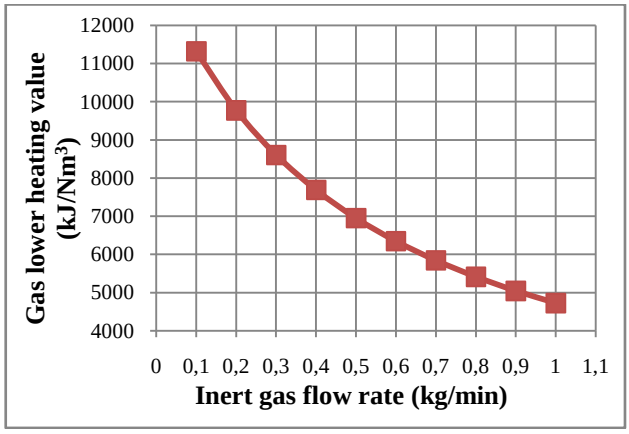

Fig. 29: gas lower heating value as a function of the inert gas flow rate.

The overall gas LHV variation over the whole interval of variation of the inert gas flow rate is considerable, going from 11324.8 kJ/Nm^3 at 0.1 kg/min to 4726.6 kJ/Nm^3 at 1 kg/min (decrease of about 58.3%).

Another negative effect coming from the increase of the inert gas flow rate, besides that already seen on the gas lower heating value, is that a resulting larger cold gas volume is entering the reactor and this obviously requires a larger heatingpower to keep its temperature constant; this means that a higher net heat duty has to be given to the reactor as it appears fromFig. 30. Indeed, from this it can be seen that the linear increase of the inert gas flow rate leads to a corresponding linear increase of the reactor net heat duty and this was quite expected. In fact, again, it is necessary to remember that the net reactor heat duty does not take into account any heat losses, but only the heat necessary to heat up the feed; it is very likely that the overall heat duty would not increase linearly if the inert gas flow rate were varied linearly, but it would show a larger build-up. The reactor net heat duty goes from 11.53 kW at 0.1 kg/min to 19.38 kW at 1 kg/min, thus showing an overall increase of about 68%.

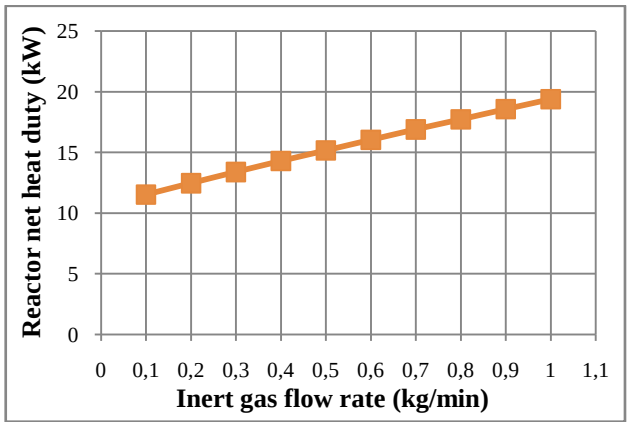

Fig. 30: reactor net heat duty as a function of inert gas flow rate.

E. Effect of the inert gas temperature

As the pyrolysis is here treated as an equilibrium process, a change of the inert gas inlet temperature will affect the energy balance on the reactor only.

Fig. 31 displays the reactor net heat duty as a function of the inert gas temperature.As one could easily expect, the reactor net heat duty exhibits a linear decreasing pattern when increasing the inert gas temperature; it goes from a value of 15.17 kW at 25 °C to 13.64 kW at 200 °C, thus showing a reduction of about 10%.

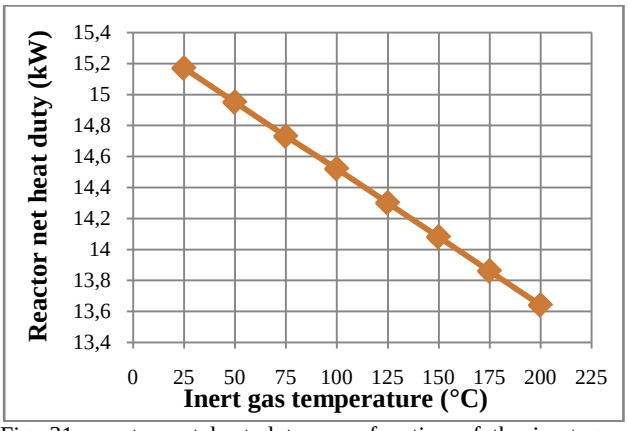

Fig. 31: reactor net heat duty as a function of the inert gas temperature.

F. Effect of the biomass feed rate

It can be noticed from Fig.32 that the main gaseous species, except for H_2O and CH_4, do not significantly change when varying the biomass feed rate. H_2O mole fraction falls from 22.89% at 10 kg/h to 8.69% at 100 kg, decreasing of about 62% while CH_4 rises from 9.14% to 19.21% (increase of about 110%); on the other hand CO and CO_2 increases are, respectively, about 22.8% and 24.2%.

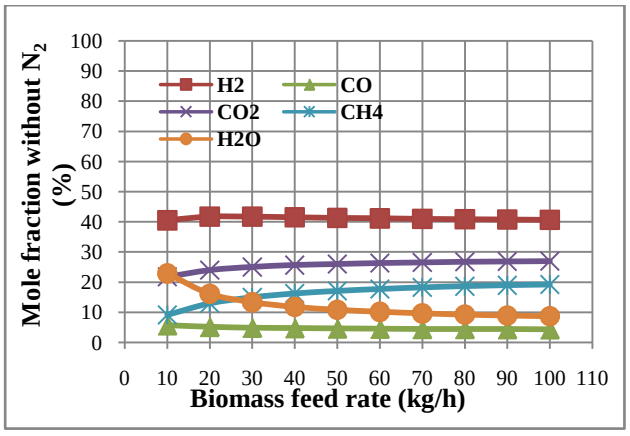

Fig. 32: mole fractions of H_2, CO, CO_2, CH_4 and H_2O in the gas product as functions of biomass feed rate.

A somewhat contradictory trend is shown by H_2, which initially grows up to a maximum at 30 kg/h of biomass flow rate and then steadily decreases. Theoretical considerations are here difficult to give, especially with reference tothe H_2pattern; anyway, one could think that the increased availability of solid carbon from the biomass feed moves reactions 2 and 3 to left and leads to larger amounts of CH_4 and CO_2 in gas phase.

The pattern of the carbon mass fraction within char when changing the biomassfeed rate can be assessed by looking at Fig. 33.

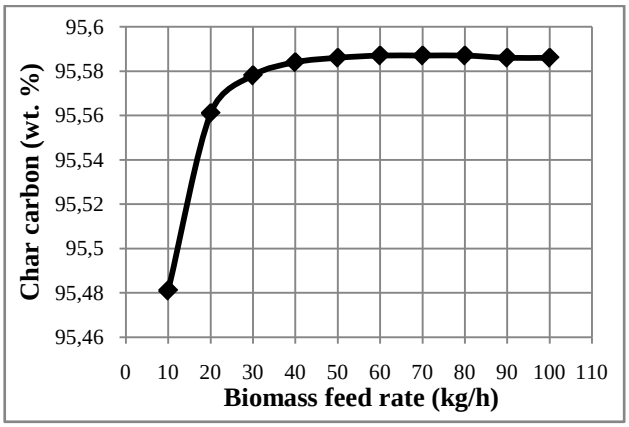

Fig. 33: char carbon mass fraction as a function of biomass feed rate.

At low values of feed rate, up to 40 kg/h, the char carbon mass fraction shows a relative rapid increase and after this point it remains more or less constant. A possible explanation for this trend could be that up to a limiting biomass feed rate the carbon within char is involved especially in reactions 2 and 3 through which it is produced together with $CO_2$and H_2O, respectively, at the expense of CO; after this point it seems that these two reactions slow down as it is witnessed by the trend of the other species involved (Fig.32). All in all, the increase in the char carbon mass fraction over the whole interval of biomass feed rate is quite limited, that is about 0.11%.

In order to assess the effect of the biomass feed rate on the mole fractions of the pollutants within the gas product the diagrams in Fig. 34 and 35 need to be observed; in fact, Fig. 34 reports a steady, slow increase in the mole fraction of H_2S,whereas NH_3 shows a maximum at 20 kg/min and then it exhibits a decreasing trend. Fig. 35, on the other hand, shows that the mole fraction of SO_2 increases with a growingbiomass feed rate.

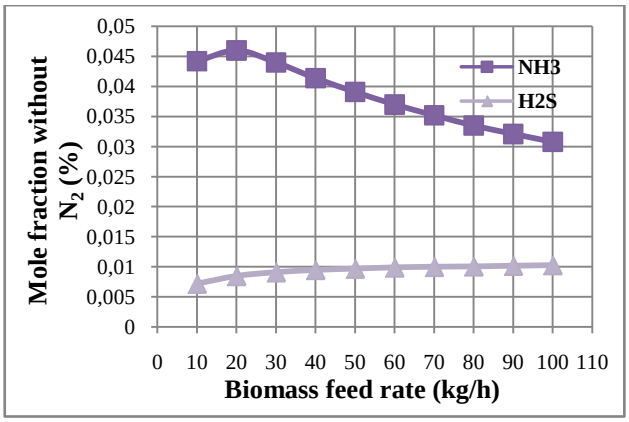

Fig. 34: NH_3 and H_2S mole fractions in the gas product as functions of feed flow rate.

The overall variations in the NH_3, H_2S and SO_2 mole fractions are approximately 34.3%, 43.1% and 77.2%, respectively.

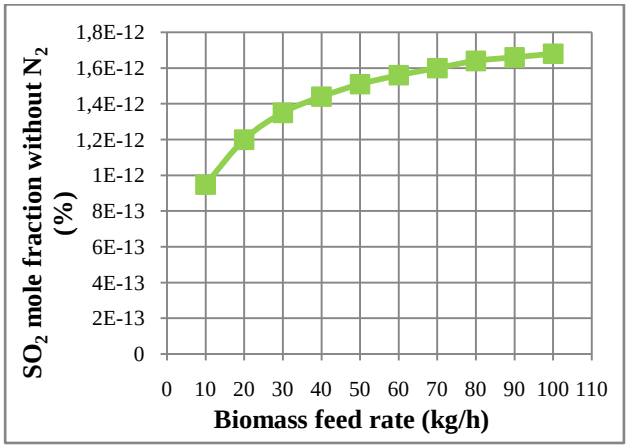

Fig. 35: SO_2 mole fraction in the gas product as a function of biomassfeed rate.

The char higher heating value, closely connected to the char carbon mass fraction through(1), increases when increasing the biomass feed rate as outlined in Fig. 36; the relative increase is more relevant at lower feed rates. Nevertheless, the absolute variation is quite limited, since it goes from 33.829 MJ/kg at 10 kg/h to 33.866 at 100 kg/h (0.1%).

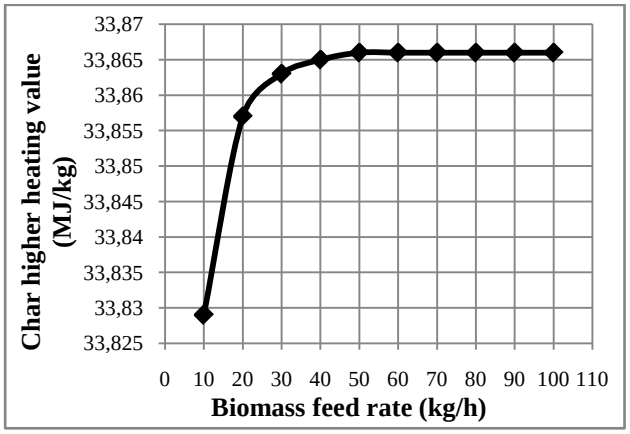

Fig. 36: char higher heating value as a function ofbiomass feed rate.

Fig. 37 shows the trend of the gas lower heating value when varying the biomass feed rate.

It is readily noticed that the gas LHV exhibits a monotonous increasing trend; this can be attributed to the increasing mole fraction of CH_4 that is reported by Fig. 32; the other two species which contribute to LHV, i.e., CO and H_2, show a decreasing trend (Fig. 32) that is balanced and overcome by that of the CH_4, thus producing a higher and higher gas lower heating value. Its increase over the whole range of variation of the biomass feed rate is quite prominent, passing from 2454.7 kJ/Nm^3 at 10 kg/h to 9151.8 kJ/Nm^3 at 100 kg/h (more than three times).

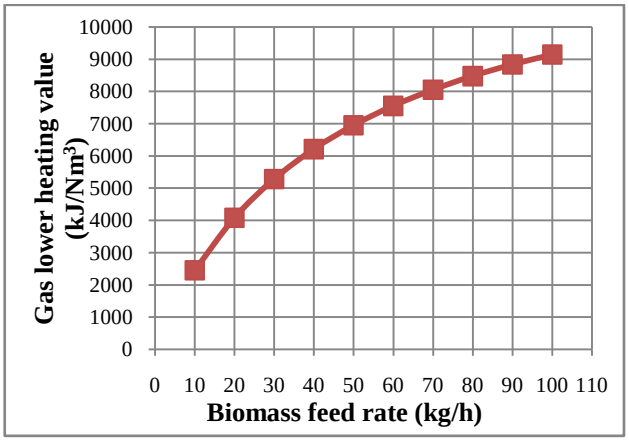

Fig. 37: gas lower heating value as a function of biomass feed rate.

Of course,the increase of the biomassfeed rate brings about changes in the reactor net heat duty as well. This is seen in Fig. 38 in which the reactor net heat duty shows a linear increase when linearly increasing the feed flow rate.

This is quite expectable because the net heat duty is linearly proportional to the amount of reacting feed; a different discussion is needed when the heat losses from the reactor are to beconsidered as they do not increase linearly with the feed rate.

The net heat duty goes from 6.2 kW at 10 kg/h to 25.86 kW at 100 kg/h (increase of more than three times).

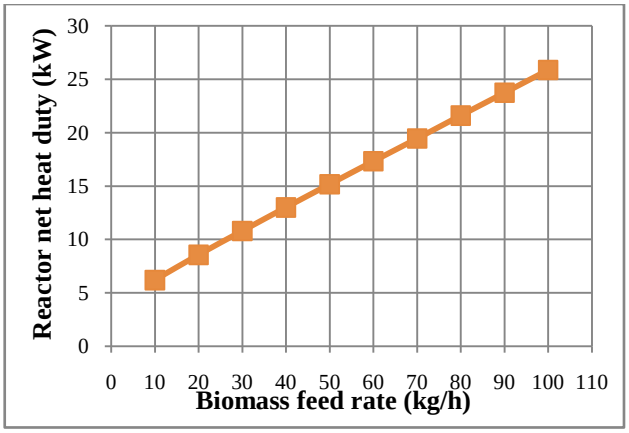

Fig. 38: reactor net heat duty as a function of feed flow rate.

G. Effect of a different feedstock

Taking advantage of the Aspen® capabilities, thetrend analysis has been further extended to consider a possible variation in the feedstock. To this end,the simulation work has been repeated for two feedstocks far different from lignocellulosic biomass, that isbrown coal and waste tyres,whose compositions have been reported in Tables I and IIas well.

The main predicted simulation results are reported in Tables V, VI, VII,VIII and IX for each feedstock as a function of the ultimate and proximate analysis data.

TableV: effects of some components of the ultimate and proximate analyses on % yields of gas, liquid and char.

	Volatile matter	Ash content	O_2 content
	52.51-70.86-84.71	1.35-5.7-6.11	0.01-24.58-43.98
Gas	62.4-51.65-71	71-62.4-51.65	51.7-62.4-71
Liquid	8.14-0.06-11.42	11.4-8.1-0.06	0.06-8.1-11.4
Char	29.5-48.3-17.61	17.61-29.5-48	48-29.5-17.6

Table VI: effects of some components of the ultimate and proximate analyses on the % mole fractions of H_2, CO, CO_2, CH_4 and H_2O in the gas.

	C content	O_2 content	Moisture content
	47.67-63.51-85.4	0.01-24.58-43.98	1.71-7.86-13.56
H_2	41.3-44.2-56.9	56.9-44.2-41.3	56.9-41.3-44.2
CO	4.64-4.31-0.29	0.29-4.31-4.64	0.29-4.64-4.31
CO_2	26.1-21.1-0.12	0.12-21.1-26.1	0.12-26.1-21.1
CH_4	17.1-18.4-37.7	37.7-18.4-17.1	37.7-17.1-18.4
H_2O	10.8-11.9-4.5	4.5-11.9-10.8	4.5-10.8-11.9

TableVII: effects of some components of the ultimate and proximate analyses on % mass fraction of char carbon.

	Ash content	O_2 content	Volatile matter
	1.35-5.7-6.11	0.01-24.58-43.98	52.51-70.86-84.71
Char carbon mass fraction	95.6-89.6-92.2	92.2-89.6-95.6	89.6-92.2-95.6

TableVIII: effects of some components of the ultimate analysis on the % mole fractions of NH_3, H_2S and SO_2 in the gas.

	S content	N content	C content	O_2 content
	0.01-0.06-0.44	0.13-0.48-1.01	47.67-63.51-85.4	0.01-24.58-43.98
NH_3	0.039-0.046-0.084	0.039-0.084-0.046	0.039-0.046-0.084	0.084-0.046-0.039
H_2S	0.0097-0.067-0.5	0.0097-0.5-0.067	0.0097-0.067-0.5	0.5-0.067-0.0097
SO_2	$1.51*10^{-12}$-$7.9*10^{-12}$-$2.51*10^{-13}$	$1.51*10^{-12}$-$2.51*10^{-13}$-$7.9*10^{-12}$	$1.5*10^{-12}$-$7.9*10^{-12}$-$2.51*10^{-13}$	$2.5*10^{-13}$-$7.9*10^{-12}$-$1.51*10^{-12}$

Table IX: effects of some components of the ultimate and proximate analyses on char HHV, gas LHV and reactor NHD.

	Ash content	O_2 content	C content	Volatile matter	Moisture content
	1.35-5.7-6.11	0.01-24.58-44	47.7-63.5-85.4	52.5-70.9-84.7	1.7-7.9-13.6
Char HHV (MJ/kg)	33.9-31.7-32.7	32.7-31.7-33.9	33.9-31.7-32.7	31.7-32.7-33.9	32.7-33.9-31.7
Gas LHV (kJ/Nm^3)	6955-6709-11379	11379-6709-6955	6955-6709-11379	6709-11379-6955	11379-6955-6709
Reactor NHD (kW)	15.2-12.4-12.9	12.9-12.4-15.2	15.2-12.4-12.9	12.4-12.9-15.2	12.9-15.2-12.4

H. Comparison with experimental results

It is very interesting to compare some of these results with those obtained through experiments by Honus[25]. In particular, the composition and volumetric flow rate of the pyrolysis gas stream have been calculated by using the Aspen simulation code under the Honus' operating conditions for the three feedstocks. Then, the predicted values have been compared to those published by Honus in Tables X and XI, respectively.

TableX: experimental and predicted mole fractions of H_2, CO, CO_2 and CH_4 at different pyrolysis temperatures from different feedstocks.

	T (°C)	Mole fractions without inert gas N_2 (%)							
		Predicted				Experimental			
		H_2	CO	CO_2	CH_4	H_2	CO	CO_2	CH_4
Biomass	500	40.4	4.29	27.4	20.0	6.4	8.7	20.3	16.4
	550	47.0	8.47	23.6	13.3	13.2	8.0	19.9	14.9
	600	50.8	14.7	18.8	8.25	18.7	12	18.3	15.4
	650	52.1	22.4	13.4	4.87	19.9	31	16.2	15.1
Brown coal	500	43.1	3.92	22.2	22.2	15.1	11	19.2	25.3
	550	50.1	7.78	19.3	14.7	19.5	10	18.3	20.7
	600	54.1	13.5	15.5	9.07	27	11	18.1	24.4
	650	554	20.6	11.0	5.35	33.9	12	16.1	14.8
Waste tyres	500	51.8	0.19	0.07	43.5	12.4	2.8	2.4	27.9
	550	65.1	0.45	0.08	30.7	13.3	3.7	2.3	19.8
	600	75.9	0.89	0.08	20.2	22.2	3.1	1.9	19.2
	650	83.6	1.47	0.06	12.8	28.3	3.9	1.4	4.6

The first observation derived from table X is that the predicted mole fractions, especially those of H_2, are sometimes far from the experimental ones: this is not surprising here because the assumption of chemical equilibrium in this work is a very strong one. Actually, in Honus' experiments the pyrolysis gases were vented whereas the pyrolizedresidues underwent a storageof about 45 minutes before discharge. Even if his process can be classified as slow pyrolysis or "gasification pyrolysis", it is still not enough to approach the chemical equilibrium.

However, even if the predicted and experimental values are far from each other, the general trends as a function of the operating variables are satisfactory, thus meaning that the predicted values are those to which the experimental ones try to tend.

TableXI: experimental and predicted volumetric gas flow rate at different pyrolysis temperatures from different feedstocks.

	T (°C)	Volumetric flow rate (m^3/s)	
		Predicted	Experimental
Biomass	500	0.006	0.00237
	550	0.00714	0.00281
	600	0.00853	0.00313
	650	0.01012	0.00352
Brown coal	500	0.00482	0.0009
	550	0.00571	0.00142
	600	0.0068	0.00145
	650	0.00803	0.00203
Waste tyres	500	0.0058	0.00178
	550	0.00638	0.00219
	600	0.00695	0.00202
	650	0.00745	0.0028

The predicted values of the volumetric gas flow rate are of the same order of magnitude of the experimental ones, but still about 2-3 times higher, as it is reported in table XI. This is again due to the assumption of chemical equilibrium, which can be approached and seldom achieved where all the volatile matter is released. Also in this case, the predicted trends as a function of the pyrolysis temperature agree with what is experimentally seen, as for the trends of the gaseous species.

IV. Conclusion

The main limiting assumption of the model developed in this work is that the residence time is considered to be long enough and the reaction rates are supposed to be fast enough to reach thermodynamic equilibrium. The comparison made of the predicted results with some experimental ones just taken as a reference has proved that even a residence time of 45 min is not enough to achieve thermodynamic equilibrium, but hours or days could be required.Unfortunately, performing pyrolysis processes with so long residence times of the feed and the inert carrier gas is too energy-demanding and out of practical interest. On the other hand, thermodynamic equilibrium calculations have the advantage of beingindependent of the flow pattern and so of the specific pyrolysis reactor design. This leads to the fact that this approach – and therefore the present Aspen© simulation model –is very versatile and can be applied for all pyrolysis systems; so, it can be used to study only the effect of the process variables while it cannot give predictions of the process equipment size.

Possible options to improve the accuracy of equilibrium-based models could be those of modifying or correcting the equilibrium model through the use of experimental results, or developing models based on quasi-equilibrium temperature approaches; in fact, these have proved to give acceptable results when applied to biomass gasification [36],[37].

Kinetic models are opposed to equilibrium models in that they describe the conversion during biomass pyrolysis, which is crucial in designing, evaluating and improving pyrolysis systems; so, they need kinetic rate expressions obtained from “ad hoc” experiments. These rate models, unlike equilibrium models, are accurate and detailed but are computationally intensive and their applicability is limited to the pyrolysis system from which the experimental kinetic information have been found.

From these considerations it is clear that the development of a universal mathematical model, capable of predicting with a good accuracy the products of a pyrolysis process of whatever feedstock in every reactor configuration, should combine the versatility of equilibrium models and the accuracy of kinetic models; this is a challenge to develop proper design procedures for pyrolysis systems. Once done, the potential of biomass as a renewable source can be further exploited all over the world to relieve the burden of the energy supply from fossil fuels and meanwhile to ease the environmental problem.

Acknowledgment

Most of the research work has been carried out in the framework of a student’s ERASMUS stay at the VŠB - Technical University of Ostrava. The EU LIFELONG LEARNING PROGRAMME is highly acknowledged for providing a scholarship.

References

[1] United Nations Environment Programme. Renewable energy: investing in energy and resourceefficiencyhttp://www.unep.org/greeneconomy/Portals/88/documents/ger/GER_6_RenewableEnergy.pdf; (2011).

[2] T. Griu, A. Lunguleasa. “Exotic and Native Species as Biomass for Renewable Energy”. *Advances in Environmental Technology and Biotechnology*, 2014,ISBN:978-960-474-384-1.

[3] V. E.Messerle, A. B.Ustimenko, O. A. Lavrichshev.“Plasma Gasification of Solid Fuels”. *Recent Advances in Energy, Environment and Economic Development*, 2012, ISBN: 978-1-61804-139-5.

[4] R. R. Riehl, C. A. Shahateet, L. S. De Souza, Dib Karam Jr. “Biomass Gasification Unit Using Sugar Cane Bagasse for Power Generation”. *Recent Advances in Energy, Environment and Economic Development*, 2012, ISBN: 978-1-61804-139-5.

[5] M. Miccio and B. Cosenza.“Fuzzy Control of a Biomass-Fired and Solar-Powered Fluidized Bed Prototype as a Residential Cogeneration System”, Proceedings (with peer review) of the 3rd Int. Conf. on Energy Systems, Environment, Entrepreneurship and Innovation (ICESEEI '14), ISSN: 2227-4359, ISBN: 978-960-474-375-9, Salerno, 17-26, June 3-5, 2014

[6] D. Mohan, C. U. Pittman, P. H. Steele. “Pyrolysis of wood/biomass for bio-oil: a critical review”. *Energy & Fuels*, Vol.20, 2006, pp. 848-89.

[7] W. Prins, B. M. Wagenaar. “Review of rotating cone technology for flash pyrolysis of biomass”. In: *Kaltschmitt M. K., Bridgwater A. V., editors. Biomass gasification and pyrolysis*. UK: CPL Scientific Ltd.; 1997. p. 316-26.

[8] G. V. C. Peacocke, A. V. Bridgwater. “Ablative plate pyrolysis of biomass for liquids”. *Biomass Bioenergy*, Vol.7, 1995, pp. 147-54.

[9] E. Heinrich, N. Dahmen, E. Dinjus. „Cost estimate for biosynfuel production via biosyncrude gasification”. *Biofuels BioprodBioref*, Vol.3, 2009, pp. 28-41.

[10] C. Wu, Z. Wang, J. Huang, P. T. Williams. “Pyrolysis/gasification of cellulose, hemicellulose and lignin for H_2 production in the presence of various nickel-based catalysts”. *Fuel*, Vol.106, 2013, pp. 697-706.

[11] J. J. M. Orfao, F. J. A. Antunes, J. L. Figuereido. “Pyrolysis kinetics of lignocellulosic materials-three independent reactions model”. *Fuel*, Vol.78, 1999, pp. 349-358.

[12] K. Raveendram, A. Ganesh, K. C. Khilar. “Pyrolysis characteristics of biomass and biomass components”. *Fuel*, Vol.75, 1996, pp. 987-98.

[13] H. Yang, R. Yan, H. Chen, C. Zheng, D. Lee. “In-depth investigation of biomass pyrolysis based on three major components: hemicellulose, cellulose and lignin”. *Energ. Fuel*, Vol.20, 2006, pp. 388-393.

[14] N. Worasuwannarak, T. Sonobe, W. Tanthapanichakoon. “Pyrolysis behaviors of rice straw, husk and corncob by TG-MS technique”. *J. Anal. Appl. Pyrol.*, Vol.78, 2007, pp. 265-271.

[15] G. Wang, W. Li, B. Li, H, Chen. “TG study on pyrolysis of biomass and its three components under syngas”. *Fuel*, Vol.87, 2008, pp. 552-558.

[16] S. Wang, X. Guo, K. Wang, Z. Luo. “Influence of the interaction of components on the pyrolysis behavior of biomass”. *J. Anal. Appl. Pyrol.*, Vol.91, 2011, pp. 183-189.

[17] E. Ranzi, A. Cuoci, T. Faravelli, A. Frassoldati, G. Migliavacca, S. Pierucci, S. Sommariva. “Chemical Kinetics of Biomass

Pyrolysis". Department Politecnico di Milano, Milano, Italy. *Energy &Fuels*, Vol.22, 2008, pp. 4292-4300.
[18] J. Piskorz, D. Radlein, D. S. Scott. "On the mechanism of the rapid pyrolysis of cellulose". *J. Anal. Appl. Pyrol*., Vol.9, 1986, pp. 121-37.
[19] J. L. Banyasz, S. Li, J. L. Lyons-Hart, K. H. Shafer. "Cellulose pyrolysis: The kinetics of hydroxyacetaldehyde evolution". *J. Anal. Appl. Pyrol.*, Vol.57, No.2, 2001, pp. 223-248.
[20] J. L. Banyasz, S. Li, J. L. Lyons-Hart, K. H. Shafer. "Gas evolution and the mechanism of cellulose pyrolysis". *Fuel*, Vol.80, No.12, 2001, pp. 1757-1763.
[21] E. M. Suuberg, I. Milosavljevic, O. Vahur. *Proc. Comb. Institute*, Vol.26, 1996, pp. 1515.
[22] T.Faravelli, A. Frassoldati, E. Ranzi, F. Hugony, G. Migliavacca. "Modellazione dettagliata della pirolisi di biomasse: Modelli cinetici di devolatilizzazione". *La Rivista dei Combustibili*, Vol.61, No.5, 2007, pp. 249-270.
[23] Aspen Tech Corporate Overview http://www.aspentech.com/corporate/press/media_kit.aspx.
[24] G. Lantagne, B. Marcos, B. Cayrol. "Computation of complex equilibria nonlinear optimization". *Comput.Chem. Eng.*, Vol.12, No.6, 1988, pp. 589-599.
S. Honus. "Gaseous components from pyrolysis – characteristics, production and potential for energy utilization". ISSN 1330-3651 (print), ISSN 1848-6339 (Online) UDC/UDK.
[25] D.-Y. Peng, D. B. Robinson."A New Two-Constant Equation-of-state". *Ind. Eng. Chem. Fundam.*, Vol.15, 1976, pp. 59–64.
[26] A. Dufour, P. Girods, E. Masson, Y. Rogaume, A. Zoulalian. "Synthesis gas production by biomass pyrolysis: effect of reactor temperature on product distribution". *International journal of hydrogen energy*, Vol.34, 2009, pp. 1726-1734.
[27] http://en.wikipedia.org/wiki/Steam_reforming
http://en.wikipedia.org/wiki/Boudouard_reaction
[28] http://en.wikipedia.org/wiki/Water_gas.
[29] H. E. Francis, W. G. Lloyd. *J.Coal Qual.*, Vol.2, No.2, 1983, pp. 21.
[30] L. Jimenez, F. Gonzalez. *Fuel*, Vol.70, No.8, 1991, pp. 947.
[31] F. Shafizadeh, W. G. Degroot. "Thermal uses and properties of carbohydrates and lignins". *New York: Academic Press*, 1976.
[32] T.Cordero, F. Marquez, J. Rodriguez-Mirasol, J. J. Rodriguez. "Predicting heating values of lignocellulosics and carbonaceous materials from proximate analysis". *Fuel*, Vol.80, 2001, pp. 1567-1571.
[33] P. M. Lv, Z. H. Xiong, J. Chang, C. Z. Wu, Y. Chen, J. X. Zhu."An experimental study on biomass air-steam gasification in a fluidized bed". *Bioresource Technology*, Vol.95, 2004, pp. 95-101.
[34] Z. A. Zainal, R. Ali, C. H. Lean, K. N. Seetharamu. "Prediction of performance of a downdraft gasifier using equilibrium modelling for different biomass materials". *Energy Convers. Manage*, Vol.42, 2001, pp. 1499-155.
[35] S. Jarugthammachote, A. Dutta. "Equilibrium modeling of gasification: Gibbs free energy minimisation approach and its application to spouted bed and spout-fluid bed gasifiers". *Energy Convers. Manage*, Vol.49, 2008, pp. 1345-1356.